DOI: 10.61782/fa.2025.0009

FORUM ACUSTICUM EURONOISE 2025

A DATA-DRIVEN TRANSFER MATRIX MODEL FOR THE DESIGN OF SAXOPHONE MOUTHPIECES

Gioele Greco[1*] **Xinmeng Luan**[2]
Alberto Bernardini[1] **Fabio Antonacci**[1] **Augusto Sarti**[1]
[1] Dipartimento di Elettronica, Informazione e Bioingegneria (DEIB), Politecnico di Milano
Piazza Leonardo Da Vinci 32, 20122 Milano, Italy
[2] Computational Acoustic Modeling Laboratory,
Center for Interdisciplinary Research in Music Media and Technology,
Schulich School of Music, McGill University, Canada

ABSTRACT

This study presents a data-driven methodology to estimate transfer matrices modeling saxophone mouthpieces based on their geometric parameters. A novel parametric model was developed to generate more than 1000 unique mouthpiece geometries. Key geometric features, such as chamber and throat cross-sections, shape radii, and baffle inclination angle, were varied to create the dataset. The training data are generated through Finite Element Method (FEM) simulations, from which transfer matrices were extracted and approximated using Chebyshev polynomials. Polynomial coefficients were then modeled using fully connected neural networks to enable efficient prediction. The results demonstrate the system's ability to accurately predict transfer matrix coefficients, highlighting the potential of computational methods to enhance the customization and design of specific elements of musical instruments, such as mouthpieces.

Keywords: *saxophone mouthpiece, acoustic modeling, finite element method, transfer matrix, data-driven design*

**Corresponding author*: *gioele.greco@polimi.it.*

1. INTRODUCTION

The saxophone mouthpiece plays a crucial role in defining the tonal characteristics and playability of the instrument [1–3]. The design of a mouthpiece involves balancing complex geometric parameters that influence airflow dynamics and, consequently, sound production [4,5]. This study focuses on the internal geometry of the mouthpiece, particularly the throat, chamber, and baffle, which significantly affect its acoustic properties [6].

Traditional evaluation methods for mouthpiece designs often rely on physical prototypes and subjective auditory assessments. These approaches are inherently time-consuming and limited in their ability to explore large design spaces [7, 8]. Recent advances in computational modeling and data-driven techniques in musical acoustics [9, 10] present new opportunities to study and optimize mouthpiece designs systematically.

In this work, we propose a parametric modeling framework for saxophone mouthpieces, enabling the automated generation of a large dataset of internal cavity geometries. Finite Element Method (FEM) simulations are employed to compute the corresponding acoustic transfer matrices (TM) for each design [**?**, 11]. Subsequently, neural networks are trained to capture the complex relationships between geometric features and the resulting acoustic responses encoded in the transfer matrices.

Furthermore, the mouthpiece models are integrated with a simplified saxophone body representation to investigate the effects of estimation errors in the transfer matrices on the overall acoustic output. This analysis provides insights into the sensitivity of the saxophone acoustics to

the geometry of the mouthpiece and the accuracy of predictive models.

The insights gained from this study provide a foundation for the design of mouthpieces customized to specific acoustic preferences, paving the way for innovations in saxophone performance and personalization [12].

2. GEOMETRIC MOUTHPIECE PARAMETERS

To establish the geometric framework for the saxophone mouthpiece, we conducted a detailed analysis of a wide range of commercially available models. Drawing on the studies of [13] and [12, 14], we identified key geometric parameters that capture the essential variations among different mouthpiece designs. The primary objective was to define a minimal yet versatile set of parameters capable of approximating a broad spectrum of mouthpiece geometries, ensuring adaptability across various styles and manufacturers.

Although this study focuses specifically on the alto saxophone mouthpiece as a representative case, the proposed methodology is generalizable and can be extended to other saxophone families, including soprano, tenor, and baritone models.

Given the large number of variables that influence mouthpiece performance, our design strategy prioritizes parameters that directly affect internal airflow and acoustic response. Based on the acoustic modeling framework presented in [15], we intentionally excluded variables associated with the reed tip interface from the parametric space. Instead, the reed channel is simplified and approximated as a rectangular window to reduce complexity and computational cost.

A geometric schematic of the internal cavity of the mouthpiece model is shown in Fig. 1. To characterize the chamber and throat, we define parameters that describe their cross-sectional dimensions and shapes. Specifically:

- the heights of the cross-sections are denoted as s_c (chamber) and s_t (throat);
- the shape radii are denoted as r_c (chamber) and r_t(throat), which determine the curvature of the cross-sections by adjusting the fillets.

For the baffle, the parameter α is introduced to represent the angle of its inclination. A lower value of α corresponds to a narrower mouthpiece, and a larger baffle is typically associated with a brighter and more focused sound. In contrast, a larger α results in a wider mouthpiece and a lower baffle, often producing a darker and warmer tone.

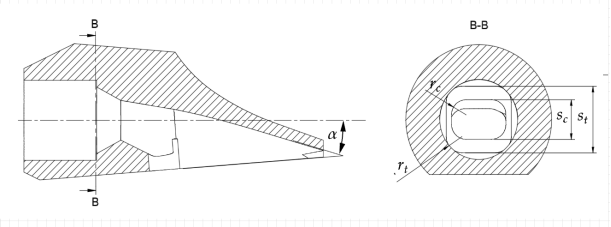

Figure 1: Scheme of the saxophone mouthpiece geometry. The left diagram shows a longitudinal cross-section highlighting the baffle angle α and internal cavity design, while the right diagram depicts the transverse cross-section (B-B plane) illustrating the chamber and throat dimensions s_c, s_t and their respective shape radii r_c, r_t.

It is important to recognize that the geometric parameters are constrained by the physical interfaces with other saxophone components, particularly the neck and the reed. Features such as the table, lay, tip opening, tip rail, and side rails must remain fixed to ensure compatibility with the wide variety of commercially available reeds. These constraints were explicitly integrated into the model to ensure that all generated geometries remain practical and compatible with standard saxophone configurations, preserving usability across a wide range of instruments and performance setups.

3. TRANSFER MATRIX METHOD

To describe the acoustic characteristics of the mouthpiece model, we employ the Transfer Matrix Method (TMM) introduced in [15]. The TMM is widely used in the study of wind instrument resonators (e.g., [11, 16, 17]), and is based on two-port acoustic theory. This theory models the reference acoustic system as a linear network with interconnected two-port elements, following the framework outlined in [15].

Specifically, a region between two ports is treated as a "black box" characterized by a 2×2 transfer matrix $\mathbf{T}(\omega)$, expressed as

$$\mathbf{T}(\omega) = \begin{bmatrix} T_{11}(\omega) & T_{12}(\omega) \\ T_{21}(\omega) & T_{22}(\omega) \end{bmatrix}, \tag{1}$$

such that the relationship between the input and output

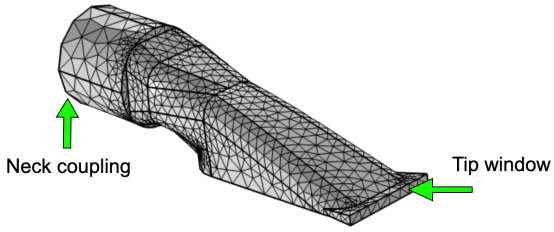

Figure 2: Finite element (FE) mesh of the saxophone mouthpiece used for acoustic analysis. The green arrows indicate the positions of the input and output ports, where acoustic pressure and volume velocity (P_i, U_i, P_o, U_o) are measured for transfer matrix derivation.

acoustic variables is given by:

$$\begin{bmatrix} P_o(\omega) \\ U_o(\omega) \end{bmatrix} = \mathbf{T}(\omega) \begin{bmatrix} P_i(\omega) \\ U_i(\omega) \end{bmatrix}. \tag{2}$$

Here, $\omega = 2\pi f$ is the angular frequency (in rad/s), while $P_i(\omega)$, $U_i(\omega)$ and $P_o(\omega)$, $U_o(\omega)$ represent the input and output acoustic pressure (in Pa) and volume velocity (in m³/s), respectively.

The transfer matrix of the mouthpiece is derived under the assumptions of linearity and passivity, which are valid when the sound source is decoupled from the mouthpiece. The reed's vibration is excluded, allowing the excitation and the nonlinearity to be modeled independently. Only propagating modes are considered, with a plane wave at the input and negligible output discontinuities. In addition, internal discontinuities are assumed to be far enough from the output plane to avoid interference. In Fig. 2 the positions of the input and output ports are shown in an example model. To derive $\mathbf{T}$, the two-load method proposed in [15] is employed. Then the following matrix equation can be solved to obtain the four terms of the TM

$$\begin{bmatrix} P_o^1 & Z_o^c U_0^1 & 0 & 0 \\ 0 & 0 & P_0^1 & Z_o^c U_o^1 \\ P_o^2 & Z_o^c U_o^2 & 0 & 0 \\ 0 & 0 & P_o^2 & Z_o^c U_o^2 \end{bmatrix} \begin{bmatrix} T_{11} \\ T_{12} \\ T_{21} \\ T_{22} \end{bmatrix} = \begin{bmatrix} P_i^1 \\ Z_i^c U_i^1 \\ P_i^2 \\ Z_i^c U_i^2 \end{bmatrix}, \tag{3}$$

where we dropped the argument ω for readability, and the superscripts 1 and 2 represent two different boundary conditions, with the loads set as a theoretical unflanged radiation impedance and the characteristic impedance, respectively.

4. DATASET CREATION

To generate a comprehensive dataset of mouthpiece parameters, we design the parametric model of the air cavity using COMSOL Multiphysics.

For our dataset, we generated five uniformly distributed values for each of s_c, s_t, and α within the predefined ranges shown in Table 1. To represent various cross-sectional shapes of the chamber, we computed three values for r_c and r_t relative to s_c and s_t using scaling factors that correspond to square, medium-smooth, and circular shapes. These parameter ranges and values, derived from [14], were informed by an analysis of the geometric characteristics of widely used commercial mouthpieces.

By combining these parameters, we obtained a dataset consisting of 1125 unique mouthpiece models. Each combination represents a plausible design variation in terms of throat and chamber shapes, as well as baffle inclinations. As an example, Fig. 3 illustrates four different mouthpiece models generated using this approach. These models demonstrate the impact of parameter variations on the throat and chamber cross-sections and the angle of the baffle.

Parameters	***Ranges Values***
s_c	[6.0 : 8.5] [mm]
s_t	[6.0 : 8.0] [mm]
α	[-5 : 25] [deg]
r_c	[0.05, 0.5, 1] $\times$ s_c
r_t	[0.05, 0.24, 0.49] $\times$ s_t

Table 1: The ranges or values of the selected geometric parameters. Five values in the ranges show in the table are randomly generated for s_c, s_t and α. Three different values with respect to each related cross section radii are generated for r_c and r_t.

4.1 Geometry Refinement

When musicians play the saxophone, it is common practice to adjust the depth of insertion of the mouthpiece into the neck to fine-tune the pitch. This mechanical coupling is critical for achieving proper intonation. To replicate this tuning behavior in our simulations, we adjust the length of

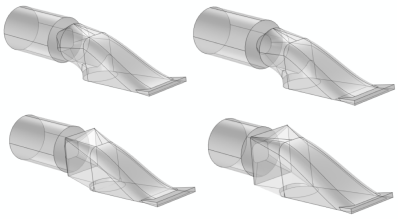

Figure 3: Four different parametric mouthpiece models obtained by different combinations of values of the selected parameters.

the coupling tube using a lumped acoustic model, ensuring that the system accurately reflects the tuning conditions.

The input impedance of the cylindrical equivalent of the mouthpiece is defined as $Z(\omega) = \frac{1}{\iota\omega\frac{\rho c^2}{V_m}}$ [15], where ι is the imaginary unit and V_m is the total volume. This relationship shows that maintaining a consistent volume of the mouthpiece in different models helps to preserve a similar resonance frequency. To match the neck diameter of the saxophone (1.7[cm] as measured on a Selmer Series III), the radius of the neck coupling's cross-section is fixed. Thus, to maintain the same volume of the mouthpiece, we adjust the length of the coupling tube accordingly.

4.2 FEM Simulation

Simulations are performed using COMSOL Multiphysics® software, employing the Pressure Acoustics, Frequency Domain finite element method (FEM) [18] to model the acoustic behavior of the air column within the saxophone mouthpiece. The accuracy and computational efficiency of this approach for wind instrument modeling have already been validated in previous studies [15].

As detailed in Section 3, two simulation scenarios are performed by applying distinct boundary conditions at the output: one with unflanged radiation impedance and the other with characteristic impedance. This setup enables the extraction of the elements of the transfer matrix necessary for subsequent acoustic analysis. A 1kPa pressure source is applied at the input tip window of the mouthpiece, depicted in Figure 2. The studied frequency range is [10,8000] Hz with a step of 50 Hz. The maximum mesh element size is $c/f_{max}/5$, with f_{max} the highest frequency.

We then extracted the TMs from the FEM simulations by solving (3), resulting in $\bar{\mathbf{T}} = [T_{ij}^{(\ell)}(\omega)] \in \mathcal{C}^{159\times1125\times4}$, where 159 is the number of sampled frequencies ω, 1125 is the number of geometry models ℓ, and we stacked them in 4 elements ij of TM $\mathbf{T}$ in (1). The obtained dataset is available at `https://kaggle.com/datasets/6c7d1b3c947d395b6d7954f9a628294e262baff0a7bee454bb119e8545ce9476`.

5. DATA-DRIVEN RECONSTRUCTION

5.1 Feedforward Neural Networks

We employed four Feedforward Neural Networks (FNN) to model the relationships between the geometric parameters and the four corresponding TM terms. The input consists of $\mathbf{x} = [s_c, s_t, \alpha, \frac{r_c}{s_c}, \frac{r_t}{s_t}]^\top \in \mathbb{R}^5$. To reduce the dimensionality of the neural network output, inspired by the approach discussed in [15], we used 10th-order Chebyshev polynomial coefficients for $\mathbf{T}$, resulting in 11 complex parameters arranged in a vector $\mathbf{p}_{ij}^{(\ell)}$. An example comparing $\mathbf{T}$ with its reconstruction from the polynomial approximation is presented in Fig. 4, demonstrating a good alignment and providing confidence in the accuracy of the polynomial fitting. For each neural network ij, the output is designed as $\mathbf{y}_{ij} = [\Re(\mathbf{p})^\top, \Im(\mathbf{p})^\top]^\top \in \mathcal{R}^{22}$, obtained by first converting $\mathbf{P}$ into a real-valued representation. The resulting vector is then normalized using the mean value across various mouthpiece models in the training dataset. Thus, given a set of geometric measurements $\mathbf{x}$, the ijth FNN must output a corresponding set of staked Chebyshev polynomial coefficients $\mathbf{y}_{ij}$ to define the ijth entry function of TM $\mathbf{T}(\omega)$.

Indeed, the dataset is divided into training, validation, and test sets with proportions of 70%, 15%, and 15%, respectively. This ensures that the model is not only trained effectively, but also evaluated for generalization on unseen data. The employed FNN architecture is shown in Fig. 5, featuring a single hidden layer with 10 neurons. The $\tanh$ activation function is used in the hidden layer to introduce nonlinearity, while no activation function is applied to the output layer. The loss function is defined as the mean squared error (MSE) between the neural network output and the exact target values $\mathbf{Y}$. The Levenberg-Marquardt backpropagation algorithm was utilized for optimization. The *MATLAB Deep Learning Toolbox* is used for the implementation.

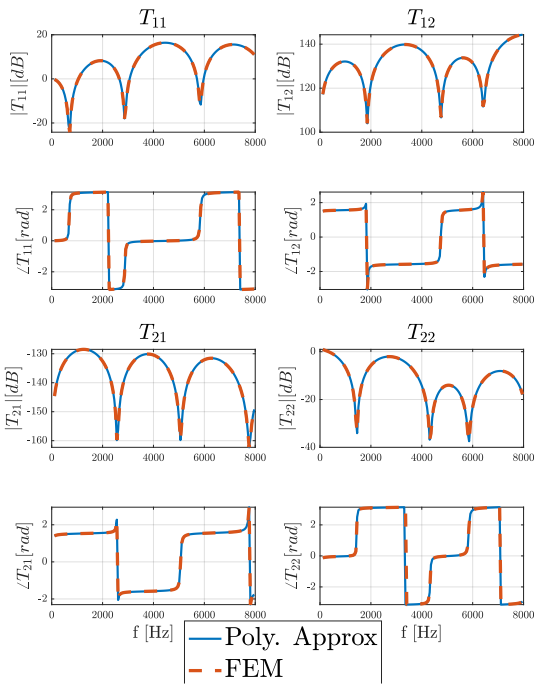

Figure 4: An example of magnitude and phase of TMs $\mathbf{T}$, comparing FEM and polynomial approximation results.

5.2 Linear Regression

As a comparison with the proposed data-driven method, we use a linear regressor. The linear regression assumes that the relationship between the dependent variable $\mathbf{Y}$ and the independent variable $\mathbf{X} = [\mathbf{x}]_\ell \; \forall \ell \in$ Training set (described in 5.1) can be expressed as

$$\mathbf{Y} = \mathbf{X}\beta + \varepsilon, \tag{4}$$

where β is the vector of regression coefficients; $\varepsilon \in \mathbb{R}^{n\times 1}$ is the vector of random errors, assumed to follow a normal distribution with zero mean and constant variance.

The vector of coefficients β can be estimated as

$$\hat{\beta} = (\mathbf{X}^T\boldsymbol{X})^{-1}\mathbf{X}^T\mathbf{Y}. \tag{5}$$

6. RESULTS

6.1 Closed Mouthpiece and Coupled System

The input impedance of the mouthpiece with a closed termination can be determined by setting the end impedance to infinity and evaluating it using the mouthpiece TM. Furthermore, to assess the influence of the mouthpiece on the saxophone body, we model the main bore of the saxophone as a truncated cone and couple it with the mouthpiece. The truncated conical resonator has an input radius of $8.05\,\mathrm{mm}$, which is equal to the radius of the mouthpiece neck coupling. The apex angle is $0.035\,\mathrm{rad}$, and the truncated cone length is $0.72\,\mathrm{m}$, which is aligned with the study in [19]. The input impedance is then derived accordingly with the unflanged radiation condition at the output. The elements of the transfer matrix for the truncated conical duct, $\mathbf{T}^{cone}$, are determined by Equation (5) in [20].

6.2 Metrics

To evaluate the performance of the proposed method, we employ three different metrics that are typically used in the literature [15]: the Normalized Mean Square Error (NMSE), the Frequency Shift (FS), and the coefficient of determination R^2.

Given a generic impedance Z_A and a ground truth impedance (i.e. Z_{FEM}) the NMSE of Z_A is defined as

$$\mathrm{NMSE}(Z_A) = ||Z_A - Z_{\mathrm{FEM}}||^2/||Z_{\mathrm{FEM}}||^2, \tag{6}$$

such that the discrepancy between estimated and reference impedance is quantified. FS expresses the deviation between the peak frequencies of two different functions and is defined as

$$\mathrm{FS}_k(Z_A) = |f_k(Z_A) - f_k(Z_{\mathrm{FEM}})|/f_k(Z_{\mathrm{FEM}}), \tag{7}$$

where k denotes the peak index and $f_k(\cdot)$ represents the resonance frequency of the magnitude peak of the given argument.

The coefficient of determination R^2 is used to evaluate the prediction accuracy. It is defined as

$$R^2 = 1 - \frac{\mathrm{SS}_{\mathrm{res}}}{\mathrm{SS}_{\mathrm{tot}}}, \tag{8}$$

where $SS_{\mathrm{res}} = \sum_{n=1}^{N}(y_n - \hat{y}_n)^2$, y_n is the value of the dependent variable for observation n, $\hat{y}_n$ is the predicted value from the model for observation n, $SS_{\mathrm{tot}} = \sum_{n=1}^{N}(y_n - \bar{y})^2$, and $\bar{y}$ is the mean of the observed values of y. R^2 values range from 0 to 1, with values closer to 1 indicating a better fit of the model to the data.

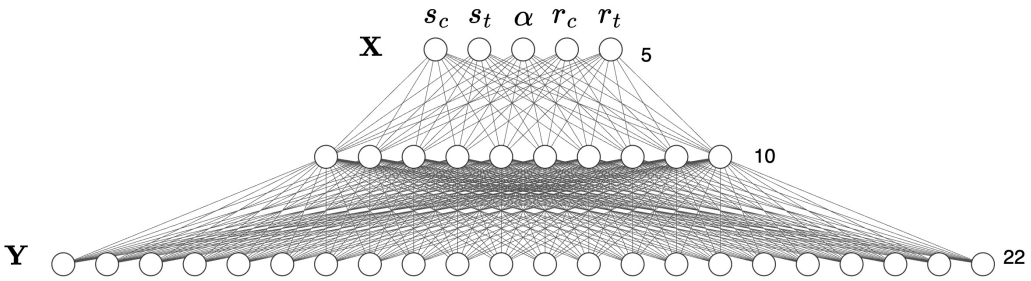

Figure 5: FNN architecture designed for modeling a single TM term.

6.3 Discussion

Performance metrics for input impedance predictions using both the FNN and linear regression models are summarized in Table 2. In all cases, the FNN consistently outperforms linear regression. Furthermore, Fig. 7 presents the coefficient of determination (R^2) for the input impedance of the coupled system, confirming the superior predictive accuracy of the FNN model.

An example of the input impedance comparison is shown in Fig. 6, where the FNN predictions closely match the FEM results, while linear regression exhibits notable deviations. These results reveal the presence of a nonlinear relationship between the mouthpiece geometric parameters and the corresponding TM elements. This underscores the importance of employing nonlinear models to adequately capture the relations between the geometric model parameters and the acoustic response.

	FNN	Linear
NMSE($\lvert Z_{in,\text{coupled}}\rvert$) [dB]	**-55.6**	-39.9
NMSE($\lvert Z_{in}\rvert$) [dB]	**-81.1**	-57.1
$\text{FS}_1(Z_{in})$ %	**0.36**	4.10
$\text{FS}_2(Z_{in})$ %	**0.24**	0.42
$\text{FS}_3(Z_{in})$ %	**0.36**	2.07
$\sum_{k=1}^{3} \text{FS}(Z_{in})/3$ %	**0.32**	2.19

Table 2: Comparison of performance metrics for FNN and Linear models, including NMSE and FS averaged for all the test dataset results.

7. CONCLUSION

In this study, we construct a synthetic dataset using a parametric model of saxophone mouthpieces that results in 1125 different designs. We consider the parameters related to the internal airflow cavity: the cross-section heights and radii of chamber and throat, and the angle of baffle inclination. The TMs of these models are then retrieved using the Finite Element Method (FEM). Additionally, a truncated cone is coupled with the parametric mouthpieces to serve as a simplified representation of the main bore of the saxophone. The acoustical influence of the mouthpiece is investigated on the basis of the input impedance spectra, which highlights the mouthpiece emphasis or modulation effect. Moreover, comparative analyses of the input impedance spectra reveal potential underlying relationships between the mouthpiece parameterization and the characteristics of the instrument. The presented dataset has significant potential for further research on the acoustic behavior of saxophone mouthpieces and sound generation. These studies can contribute to advances in the design of saxophone mouthpieces.

8. ACKNOWLEDGMENTS

We would like to acknowledge the Multilayered Urban Sustainability Action (MUSA) project, which is funded by the European Union, for their contributions to this work.

9. REFERENCES

[1] S. Carrala, V. Lorenzonib, and J. Verlindenc, "Influence of mouthpiece geometry on saxophone playing," *Proceedings of the Third Vienna Talk on Music Acoustics*, vol. 16, p. 19, 2015.

[2] A. H. Benade, *Fundamentals of musical acoustics*. Courier Corporation, 1990.

[3] V. R. Hasbrook, *Alto saxophone mouthpiece pitch and its relation to jazz and classical tone qualities*. PhD

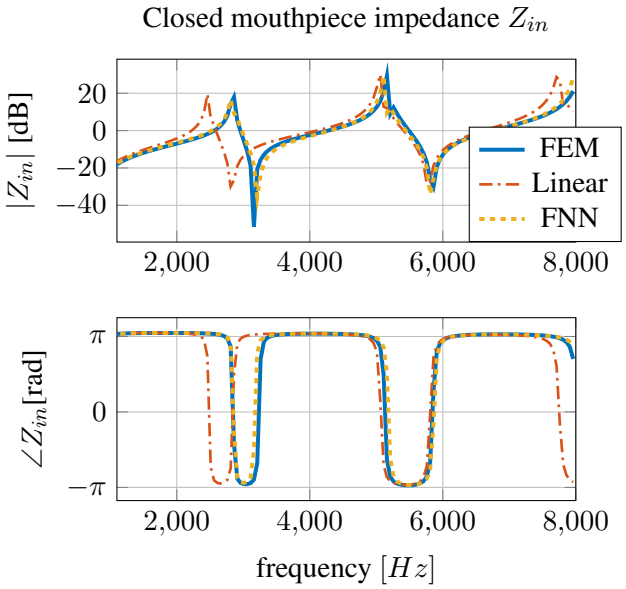

Figure 6: Example of input impedance magnitude (top) and phase (bottom) for the closed mouthpiece configuration. Results from the FEM simulation are shown alongside predictions from the linear regression model and the FNN. The FNN closely replicates the FEM results across the frequency range, while the linear model exhibits significant deviations, particularly around resonance and anti-resonance frequencies.

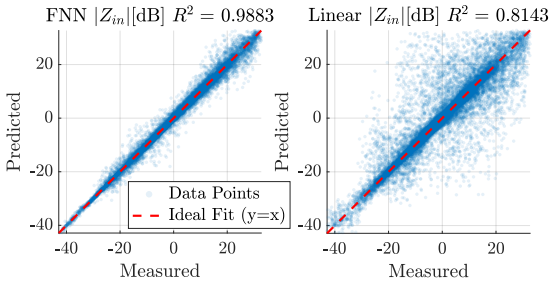

Figure 7: Comparison of predicted versus measured input impedance magnitudes (in dB) for the FNN, left and linear regression model (right) across all mouthpiece geometries. The FNN demonstrates a significantly higher coefficient of determination ($R^2 = 0.9883$), closely aligning with the ideal $y = x$ reference (red dashed line), while the linear model exhibits reduced accuracy ($R^2 = 0.8143$) and greater dispersion from the ideal fit.

thesis, University of Illinois at Urbana-Champaign, 2005.

[4] V. Lorenzoni and D. Ragni, "Experimental investigation of the flow inside a saxophone mouthpiece by particle image velocimetry," *The Journal of the Acoustical Society of America*, vol. 131, no. 1, pp. 715–721, 2012.

[5] S. Wang, G. Scavone, and E. Maestre, "Two methods for acoustic modeling of the saxophone mouthpiece," *The Journal of the Acoustical Society of America*, vol. 148, pp. 2611–2611, 10 2020.

[6] J. Kergomard, P. Guillemain, P. Sanchez, C. Vergez, J.-P. Dalmont, B. Gazengel, and S. Karkar, "Role of the resonator geometry on the pressure spectrum of reed conical instruments," 2019.

[7] A. Ricardo da Silva, G. P. Scavone, and M. van Walstijn, "Numerical simulations of fluid-structure interactions in single-reed mouthpieces," *The Journal of the Acoustical Society of America*, vol. 122, no. 3, pp. 1798–1809, 2007.

[8] T. Yoshinaga, H. Yokoyama, T. Shoji, A. Miki, and A. Iida, "Global numerical simulation of fluid-structure-acoustic interaction in a single-reed instrument," *The Journal of the Acoustical Society of America*, vol. 149, no. 3, pp. 1623–1632, 2021.

[9] D. G. Badiane, S. Gonzalez, R. Malvermi, F. Antonacci, and A. Sarti, "A neural network-based method for spruce tonewood characterization," *The Journal of the Acoustical Society of America*, vol. 154, no. 2, pp. 730–738, 2023.

[10] J.-F. Petiot, M. Roatta, V. Fréour, and K. Arimoto, "Contribution of machine learning and physics-based sound simulations for the characterization of brass instruments," in *Forum Acusticum 2023*, 2023.

[11] G. P. Scavone, "A tutorial on the transfer matrix

method for acoustic modeling," *Journal of the Acoustical Society of America*, vol. 149, 2021.

[12] V. Lorenzoni, E. Doubrovski, and J. Verlinden, "Embracing the digital in instrument making: Towards a musician-tailored mouthpiece by 3d printing," pp. 419–424, s.n., 2013.

[13] F. S. Wyman, *An acoustical study of alto saxophone mouthpiece chamber design*. University of Rochester, 1972.

[14] M. Ozdemir, V. Chatziioannou, J. Verlinden, G. Cascini, and M. Pàmies-Vilà, "Towards 3d printed saxophone mouthpiece personalization: Acoustical analysis of design variations," *Acta Acustica*, vol. 5, p. 46, 2021.

[15] S. Wang, E. Maestre, and G. Scavone, "Acoustical modeling of the saxophone mouthpiece as a transfer matrix," *The Journal of the Acoustical Society of America*, vol. 149, no. 3, pp. 1901–1912, 2021.

[16] A. Dell, A. Krynkin, and K. Horoshenkov, "The use of the transfer matrix method to predict the effective fluid properties of acoustical systems," *Applied Acoustics*, vol. 182, p. 108259, 2021.

[17] K. Verdière, R. Panneton, S. Elkoun, T. Dupont, and P. Leclaire, "Prediction of acoustic properties of parallel assemblies by means of transfer matrix method," *Proceedings of Meetings on Acoustics*, vol. 19, p. 065011, 05 2013.

[18] O. C. Zienkiewicz and P. Morice, *The finite element method in engineering science*, vol. 1977. McGraw-hill London, 1971.

[19] J.-B. Doc, C. Vergez, P. Guillemain, and J. Kergomard, "Sound production on a "coaxial saxophone"," *The Journal of the Acoustical Society of America*, vol. 140, no. 5, pp. 3917–3924, 2016.

[20] A. Lefebvre, G. P. Scavone, and J. Kergomard, "External tonehole interactions in woodwind instruments," *Acta Acustica united with Acustica*, vol. 99, no. 6, pp. 975–985, 2013.